Journal of Power Sources 264 (2014) 92–99

Contents lists available at ScienceDirect

Journal of Power Sources

journal homepage: www.elsevier.com/locate/jpowsour

Deformation of PEM fuel cell gas diffusion layers under compressive loading: An analytical approach

Vahid Norouzifard*, Majid Bahrami

Laboratory for Alternative Energy Conversion (LAEC), Mechatronic Systems Engineering, Simon Fraser University, BC V3T 0A3, Canada

HIGHLIGHTS

- A new mechanistic model has been developed to predict the PEMFCs GDL's behavior under compression.
- Unit cell approach has been utilized to model the GDL's complex microstructure.
- The model takes into account microstructural parameters and properties of the fibrous porous medium.

ARTICLE INFO

Article history:
Received 9 October 2013
Received in revised form
12 March 2014
Accepted 10 April 2014
Available online 24 April 2014

Keywords:
Gas diffusion layer
Porous media
Fuel cell
Beam theory
Mechanical behavior
Compression

ABSTRACT

In the PEM fuel cell stack, the fibrous porous gas diffusion layer (GDL) provides mechanical support for the membrane assembly against the compressive loads imposed by bipolar plates. In this study, a new mechanistic model is developed using fundamental beam theory that can accurately predict the mechanical deflection of GDL under compressive loads. The present analytical model is built on a unit cell approach, which assumes a simplified geometry for the complex and random GDL microstructure. The model includes salient microstructural parameters and properties of the fibrous porous medium including: carbon fiber diameter, fiber elastic modulus, pore size distribution, and porosity. Carbon fiber bending is proved to be the main deformation mechanism at the unit cell level. A comprehensive optical measurement study with statistical analysis is performed to determine the geometrical parameters of the model for a number of commercially available GDL samples. A comparison between the present model and our experimental stress–strain data shows a good agreement for the linear deformation region, where the compressive pressure is higher than 1 MPa.

1. Introduction

A proton exchange membrane (PEM) fuel cell consists of a five-layered structure called the membrane electrode assembly (MEA), which is sandwiched between bipolar plates [1]. The gas diffusion layer (GDL), one of the main components in the membrane electrode assembly (MEA), is a carbon fiber based highly porous media in the form of paper or cloth. Fig. 1 shows microstructure of a GDL captured by scanning electron microscope (SEM). The main duties of the GDL in a fuel cell stack include: acting as a mechanical support, providing electronic conductivity between components, providing reactant access to catalyst layers as well as removing generated heat and reaction products [2]. To collect generated electricity and heat from the cell, an appropriate contact between the membrane layers with low thermal and electrical contact resistances is essential. To insure proper contact between layers and also to seal the cell, the MEA layers are compressed between the bipolar plates by an initial normal pressure applied during the assembling process. In addition to the assembly pressure, extra compressive loads are applied on the GDL during the fuel cell operation due to hygro-thermal loading and membrane swelling [3–9]. The flexible, porous microstructure of the GDL deforms considerably when subjected to such compressive loadings. The deformation results in significant changes in the GDL's properties such as porosity, permeability, diffusivity, electrical and thermal bulk conductivities and contact resistances [1]. These property changes can significantly impact the transport phenomena, overall performance and life of the fuel cell stack. Therefore, the mechanical behavior of GDL under compression must be understood. In recent years, a number of studies have focused on the experimental and analytical investigation of the mechanical [10–15] as well as thermal [2,16–19] and electrical [11] behavior of the GDL and its interfacial interaction [1,2,17,20–23] under compressive loading.

* Corresponding author.
E-mail addresses: v.norouzi.fard@gmail.com (V. Norouzifard), mbahrami@sfu.ca (M. Bahrami).

http://dx.doi.org/10.1016/j.jpowsour.2014.04.057
0378-7753/

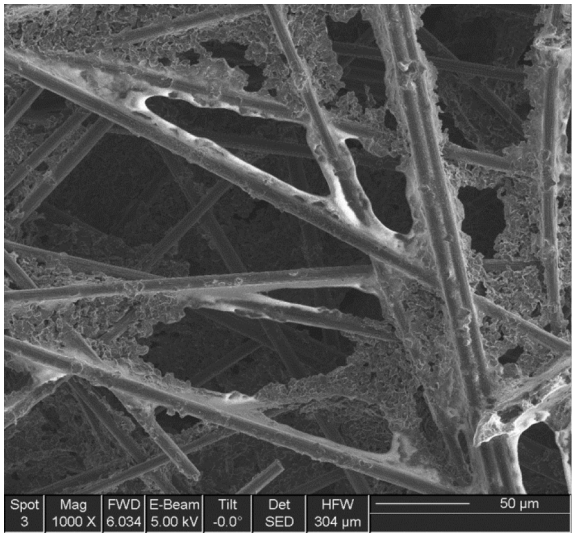

Fig. 1. SEM image of the fibrous microstructure of a PEMFC gas diffusion layer, GDL: SIGRACET SGL 24 BA.

The majority of the existing studies on the GDL's mechanical deformation were focused on numerical simulation of inhomogeneous compression of GDL under the bipolar plates' ribs using finite element method (FEM) [1,6,8,24–26]. In all of these studies, commercial FEM software was utilized for mechanical modeling. Due to the high porosity (78% and higher), GDLs show a nonlinear mechanical behavior in through plane compression. To develop a more realistic FEM model for GDL in the fuel cell, Garcia-Salaberri et al. [1] created an empirical nonlinear stress–strain relationship by curve fitting widespread data sets available in the literature. Although such empirical relationships can resolve the FEM models requirements, they do not explain the dependency of the mechanical behavior as a function of the GDL microstructure.

Developing a reliable mechanical model that can accurately predict the behavior of the GDL under compressive loads by considering its salient porous microstructure properties will provide an accurate stress–strain relationship for the GDL deformation during compression and increase the accuracy of FEM simulations. Moreover, the mechanical model will be useful to model the GDL bulk and interfacial transport phenomenon in the MEA.

Xing et al. [27] determined an optimum clamping pressure around 0.77 MPa for SGL 10 BB GDL type and operating voltage of 0.7 V and concluded that the optimum clamping pressure will increase when the operating voltage increases. Therefore, depending on the fuel cell operating condition, the operating pressure can be higher than 0.8 MPa. GDL compression test data [10,11,28] shows a compression modulus that increases from a small value, then, beyond a critical pressure remains constant. Nitta [28] determined compressive stress of 1 MPa to be the critical stress for SGL 10 BA GDL and related the linear deformation region between pressures 1–3.5 MPa to the crushing of the hydrophobic pores in the GDL. Our study focuses on the modeling of the GDL mechanical behavior in pressures higher than 1 MPa, which is the operation pressure range of PEM fuel cells in high operating voltages. We plan to address the stress range below 1 MPa in our future study.

In this paper, we develop a new mechanistic analytical model that predicts the compressive stress–strain relationship of carbon paper GDLs from their microstructural parameters such as fiber diameter and elastic modulus, pore size distribution and porosity. A unit cell approach is used in which the random, complex microstructure of real materials is modeled by a simplified geometry that is assumed to be repeated throughout the media. The unit cell approach has been successfully used by our group for modeling GDL's thermal conductivity, thermal contact resistance, and permeability [2,18,29,30]. Fundamental beam bending theory is used to model carbon fiber bending as the main deformation mechanism at the unit cell level and the overall GDL deformation is calculated from the summation of all unit cells' deformations. To determine the effective unit cell length, the distance between adjacent fiber intersections and pore area are measured optically at random locations on several off-the-shelf sample GDLs. The effective unit cell length is determined using a statistical analysis by calculating parameters such as the mean standard deviation and coefficient of variation of each GDL sample.

2. Analytical model development

Paper-based carbon fiber GDLs have a fibrous layered structure in which each layer consists of randomly distributed carbon fibers. Based on the deformation mechanism of the structure, an appropriate geometrical model is needed to represent the random and complex structure of the GDL as simply as possible. Fig. 2 shows the proposed unit cell for the GDL modeling, the same unit cell has been used consistently in our previous GDL thermal [2,18] and permeability models [29,30]. This simple geometric model includes all the salient GDL microstructural characteristics needed to capture the mechanical behavior under compression. As shown in Fig. 2, each fiber acts as a bending beam in which the fibers below and above the contact spot act as the supports and concentrated forces, respectively. Each fiber in a unit cell can be divided into small parts with two supports at the ends and one concentrated load in between, see the dashed line in Fig. 2c. Based on the interaction between neighboring unit cells, the boundary condition shown in Fig. 2d can be considered with good approximation. Deflection of the unit cell beam, δ, under a specified load, F, can be determined by the well-known beam bending theory [31] as:

$$\delta = \frac{64Fl^3}{3\pi Ed^4}\left(-n^6+3n^5-3n^4+n^3\right) \tag{1}$$

where, l, E and d are the unit cell length, carbon fibers elastic modulus in longitudinal direction and fiber diameter, respectively and n is the fraction that shows the location of the bending load on the beam, as shown in Fig. 3. n is a random parameter and its value varies between zero and one. Therefore, the average value of $f(n) = -n^6+3n^5-3n^4+n^3$ for $0 \le n \le 1$ can be calculated by integration of f. Substituting the average value of f in Eq. (1) gives:

$$\delta = \frac{16Fl^3}{105\pi Ed^4} \tag{2}$$

A mechanical model is needed to relate the GDL total deformation to the unit cell deflection. Fig. 3 presents a schematic of the GDL layered structure under compressive loads in which the layers act as stacked disc springs each of which has an effective stiffness of k_l. Assuming equal stiffness for all layers of GDL, the total through thickness deformation of GDL can be written as:

$$\delta_{GDL} = \sum_{1}^{M}\delta_l = \frac{MF}{k_l} \tag{3}$$

where, δ_l and M are the layer deformation and number of the GDL layers, respectively. The number of layers, M, can be obtained from the GDL thickness and fibers diameter, by:

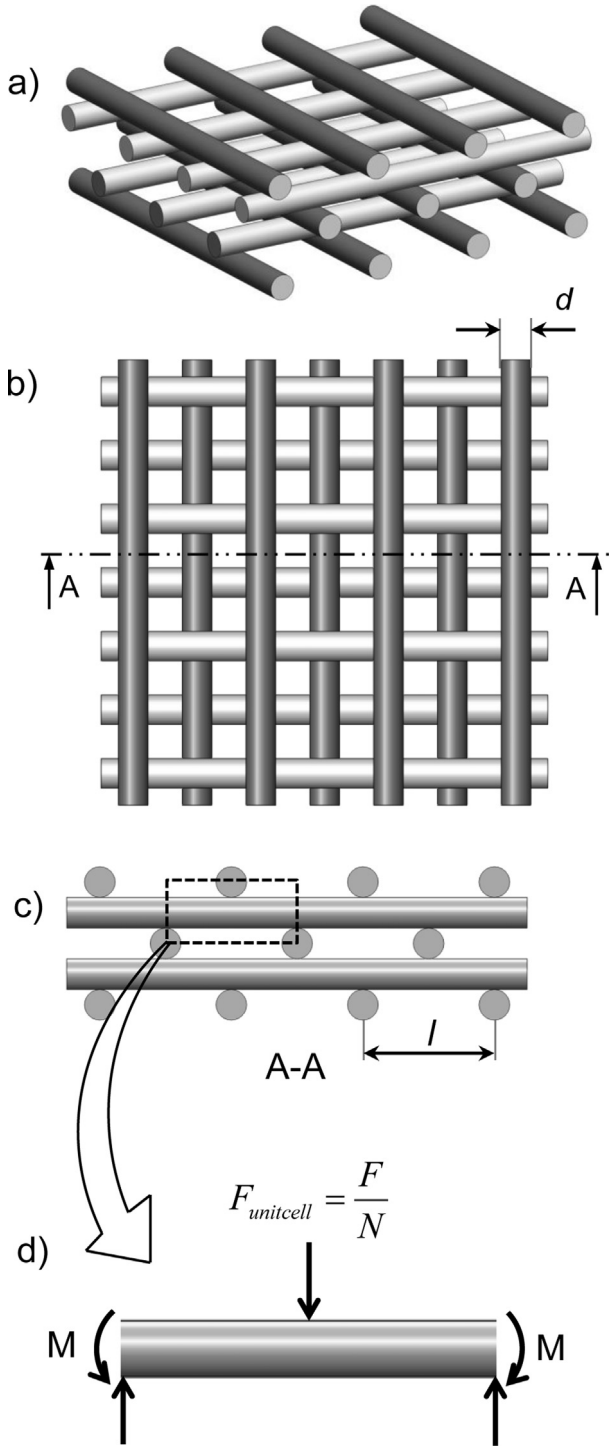

Fig. 2. Schematics of the proposed geometrical model for the GDL (a) isometric view, (b) top view, (c) cross-view section and (d) unit cell beam and boundary condition.

$$M = \frac{t}{d} \tag{4}$$

As shown in Fig. 3, each layer is composed of unit cell beams that act as parallel springs under compressive load. Therefore, the stiffness of a GDL layer is equal to the summation of the unit cells stiffness. Using Eq. (2) to calculate the stiffness of the unit cell, the effective stiffness of a GDL layer is calculated as:

$$k_{\mathrm{l}} = \sum_{1}^{N} k_i = \frac{105\pi E}{16} \sum_{1}^{N} \frac{d_i^4}{l_i^3} \tag{5}$$

where, N and l_i are the number and length of the unit cell beams in each layer, respectively. N is estimated by calculating the number of pores in one layer. Microscopic images show that both N and l_i have random distributions and vary throughout GDL layers. In this paper, a comprehensive optical study is performed to estimate the appropriate number of measurements needed to statistically determine the effective unit cells length using a microscope, as shown in sample images presented in Fig. 4. A random distribution is found for the effective unit cell length for GDL samples studied, which will be presented in the following section. Correlation between statistical parameters of independent random variables with their simple algebraic products can be found in the literature [32], therefore, the summation appeared in Eq. (5) can be calculated using the statistical parameters of unit cell length distribution such as mean value and coefficient of variation as:

$$\sum_{1}^{N} \frac{d_i^4}{l_i^3} = N\mu_{\frac{d^4}{l^3}} = N\frac{\mu_d^4}{\mu_l^3}\left(1+6C_{\mathrm{l}}^2\right)\left(1+6C_{\mathrm{d}}^2\right) \tag{6}$$

where, μ and C are the random variable mean and coefficient of variation, l and d are indices for the unit cell length and fiber diameter, respectively. Appendix A shows the derivation of Eq. (6). Using the GDL geometrical model presented in Fig. 2, each pore is composed of four unit cell beams that belong to two neighboring layer. Therefore, each pore has two unit cells from the same layer and shares fibers with the neighbor pores. Thus, the total number of unit cells in each layer can be estimated by the total number of pores in the layer. Considering that the summation of all pore areas and the area occupied by fibers should be equal to the sample area, the number of unit cells in one layer can be calculated as:

$$N = \frac{A_{\mathrm{s}}\varepsilon}{\mu_{A_{\mathrm{pore}}}} \tag{7}$$

where, A_{s}, ε and $\mu_{A_{\mathrm{pore}}}$ are the sample area, porosity, and pore area mean value, respectively. Substituting Eqs. (4)–(7) into Eq. (3) gives:

$$\delta_{\mathrm{GDL}} = \frac{16tF\mu_{\mathrm{l}}^3\mu_{A_{\mathrm{pore}}}}{105\pi E\mu_{\mathrm{d}}^5 A_{\mathrm{s}}\varepsilon\left(1+6C_{\mathrm{l}}^2\right)\left(1+6C_{\mathrm{d}}^2\right)} \tag{8}$$

After non-dimensionalization of Eq. (8), a new compact relationship between the compressive strain, e, and stress, σ, is obtained as follows:

$$e = \frac{16\sigma}{105\pi E}\left(\frac{l}{d}\right)_{\mathrm{eff}}^5 \tag{9}$$

where

$$\left(\frac{l}{d}\right)_{\mathrm{eff}} = \left(\frac{\mu_l^3\mu_{A_{\mathrm{pore}}}}{\varepsilon\mu_{\mathrm{d}}^5\left(1+6C_{\mathrm{l}}^2\right)\left(1+6C_{\mathrm{d}}^2\right)}\right)^{\frac{1}{5}} \tag{10}$$

In the next section, the developed analytical results are compared with our and others' experimental data.

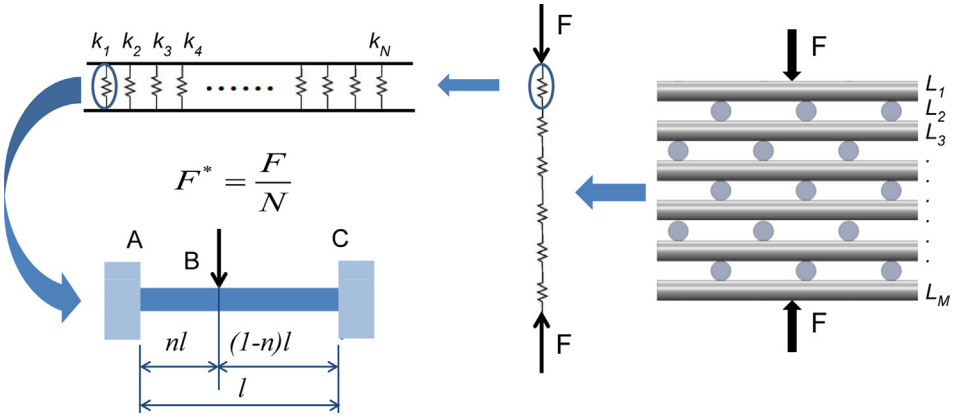

Fig. 3. GDL mechanical deformation model schematic.

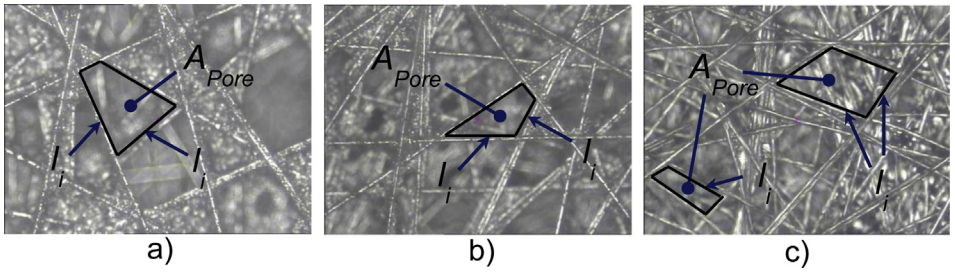

Fig. 4. Microscopic image of (a) SGL SEGRACET 25 AA, (b) SGL 24 AA, and (c) TGP-H-60 GDL samples with 92, 88, and 78% porosity, measurement of the unit cell length and pore area between fibers.

3. Results and discussion

3.1. Statistical measurements

As seen in Eqs. (8) and (10), to model the GDL mechanical deformation, the mean and standard deviation of the geometrical parameters of the microstructure are needed, including the distance between two adjacent intersections between fibers (called the unit cell beam length in the present study), fiber diameter, and pores area. It should be noted that the microstructure parameters of the GDL varies from manufacturer to manufacturer, thus, optical (microscopic) measurements and the statistical analysis should be performed for each new material. Fig. 4 shows an optical image taken from GDL samples: SGL SEGRACET 24AA and 25AA, and Toray TGP-H-60; the unit cell lengths and pore area are marked. In order to determine a sufficient number of measurements for each sample, a sensitivity analysis is performed. We systematically increased the number of optical measurements by increments of 150 and calculated the variation of the mean and standard deviation. Figs. 5 and 6 show the unit cell length mean and the standard deviation versus the number of optical measurements for SGL 24AA and 25AA, and Toray TGP-H-120 GDL samples. As seen in Figs. 5 and 6, the value of both statistical parameters plateau after approximately 600 random optical measurements, beyond this, the average value of both parameter values becomes independent from the statistical population size. The probability density of the measured data versus unit cell length is presented in Fig. 7 for two commercially available GDL samples SGL 25AA and SGL 24AA. All the measured statistical and previously reported properties as well as other geometrical characteristics of the SIGRACET SGL 24AA, 25AA, and 10 BA and Toray TGP-H-060 and TGP-H-120 GDLs needed in the present model, Eqs. (9) and (10), are listed in Table 1.

3.2. Model validation

To validate the present model, compression tests were performed on commercially available SEGRACET SGL 24AA and 25AA. The results of compression tests on TORAY TGP-H-60 and TGP-H-120 GDL samples previously performed in our group [2] and SEGRACET SGL 10 BA data from literature [28] were also used in model validation. Fig. 8 shows the schematic of the experimental apparatus used to perform compression tests on the GDL samples. The machine was originally designed for the thermal contact resistance

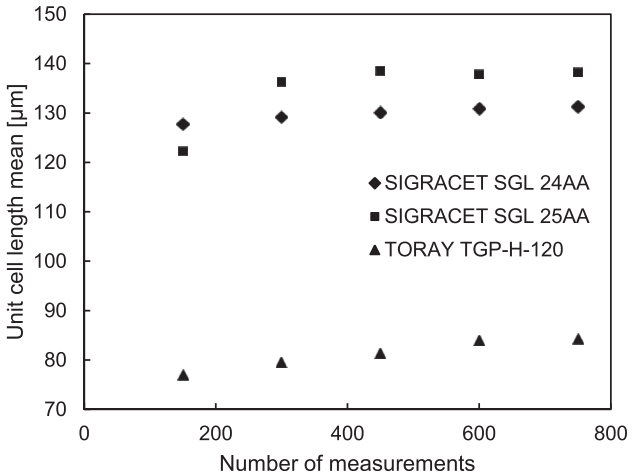

Fig. 5. Measured mean value for unit cell length versus number of optical measurements for SGL 24 AA, SGL 25 AA and TORAY TGP-H-120 GDLs.

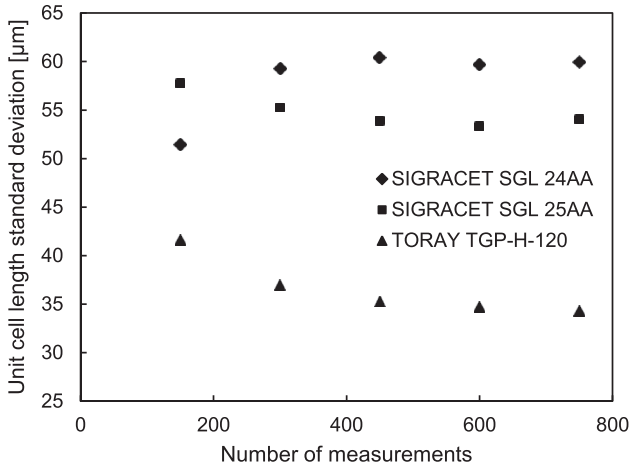

Fig. 6. Standard deviation of unit cell length versus number of measurements for SGL 24 AA, SGL 25 AA and TORAY TGP-H-120 GDLs.

and thermal conductivity measurements [17]. This apparatus is equipped with an Acuity AR 700 laser displacement sensor and A-Tech LBO-2K load cell to measure the deformation and compressive load, respectively. As shown in Fig. 8, applied load by a hydraulic jack on the test column causes compressive deformation in the GDL sample sandwiched between flux meters. The laser sensor measures the upper flux meter displacements by 0.1 μm resolution during the loading of the samples. The GDL samples are cut in circular shape with a 25 mm diameter. Figs. 9 and 10 show the stress–strain diagrams for SIGRACET and Toray GDL samples used for model validation in the present study. Our GDL compression test results (Fig. 9) are consistent with the available data in the literature [10,11,28], i.e., GDL thickness compression modulus starts with a small value in lower pressure range and increases until the compressive stress reaches 1 MPa range. It remains constant above 1 MPa pressure. Nitta [28] related the linear deformation region between pressures 1–3.5 MPa to the crushing of the hydrophobic pores in the GDL. In order to compare the predicted results with experimental data, it is necessary to assign a value for C in the model equation presented in Figs. 9 and 10. Root mean squares of difference between the model predicted and experimentally measured stresses under various strains are calculated by $E_{\mathrm{rms}} = \sqrt{\sum(\sigma_{\mathrm{exp.}} - \sigma_{\mathrm{model}})^2}$. Value of C is determined by minimizing E_{rms}. Values of C corresponding to the studied GDLs in this paper are listed in Table 1. As shown in Table 1, the variation in C is small for the GDL types from the same manufacturer and the model is not sensitive to C. As such, an average value for $C = 1.07$ and $C = 1.32$ can be used for SEGRACET and TORAY GDLs, respectively. As can be seen in Figs. 9 and 10, the present model captures the deformation trend in the higher pressure range and successfully predicts the GDL mechanical behavior for the compressive pressures higher than 1 MPa.

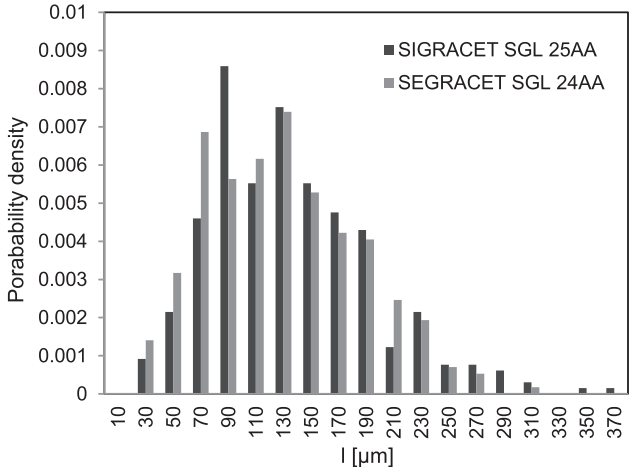

Fig. 7. Probability density of the measured data versus unit cell length for SGL 25AA and SGL 24AA samples.

The effective compression modulus of the GDL can be defined as:

$$E^* = \frac{\mathrm{d}\sigma}{\mathrm{d}e} \tag{11}$$

combining Eq. (9) and (11) gives:

$$E^*_{\mathrm{Model}} = \frac{105\pi E}{16\left(\frac{l}{d}\right)^5_{\mathrm{eff}}} \tag{12}$$

The measured effective compression modulus of the tested GDLs is compared with the analytically predicted compression modulus in Fig. 11. The GDL shows a nonlinear mechanical behavior in the pressures less than 1 MPa in which the effective compression modulus and the slope of the stress–strain diagram increase continuously (see Fig. 11). One potential reason for this nonlinear behavior could be the existence of 'gaps' and binder material between the fibers in the GDL microstructure. In fact, in the low pressure range the gaps between fibers lead to larger values for the unit cell beam length than optically measured data. It should be noted that the layers stiffness decreases as the unit cell length increases, as shown in Fig. 12. The effective non-dimensionalized unit cell length ($l\ d^{-1}$) calculated by substituting the GDL optically measured microstructural parameters in Eq. (10) and the experimental stress–strain data in Eq. (9) are compared in Fig. 12. As the compressive modulus, the effective non-dimensionalized unit cell length ($l\ d^{-1}$) converges to the experimental data in the compressive pressures higher than 1 MPa, as seen in Fig. 12. Fig. 13 schematically shows the concept of 'gaps' used to explain this low pressure deformation behavior using the unit cell effective length. In Fig. 13, the solid and dashed lines show the fiber deflections before and after compression in the low range pressure (<1 MPa), respectively. Also the bent fiber deformation fills the gap between the fibers, thus the effective unit cell length is changed. As previously mentioned, the focus of the present study is the modeling of the GDL mechanical behavior under compression pressure above 1 MPa; the nonlinear region (pressure <1 MPa) will be addressed in our future study. Also, Fig. 12 shows that the proposed model has the capability to predict the effective unit cell length of various GDL types. The effective unit cell length can be calculated from the results of GDL compression tests with ±2% of accuracy.

Table 1
The mechanical properties and geometrical characteristics of the SIGRACET and TORAY GDL samples used in this study.

GDL type	ε (%)	μ_l (μm)	C_l	$\mu_{A_{\mathrm{pore}}}$ (μm^2)	μ_d (μm)	C_d	E (GPa) [34]	C
SGL 24AA	88 [18]	130	0.414	9091	6.95	0.0812	225	−1.07
SGL 25AA	92 [18]	135.8	0.433	11,284	6.95	0.0812	225	−1.12
SGL 10BA	88 [28]	118.5	0.376	8949	6.95	0.0812	225	−1.02
TGP-H-060	78 [18]	97.24	0.387	6870	6.13	0.106	225	−1.35
TGP-H-120	78 [18]	83.95	0.413	6357	6.13	0.106	225	−1.30

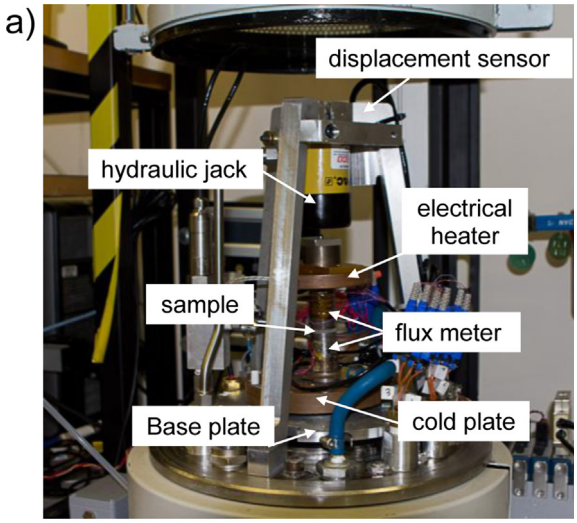

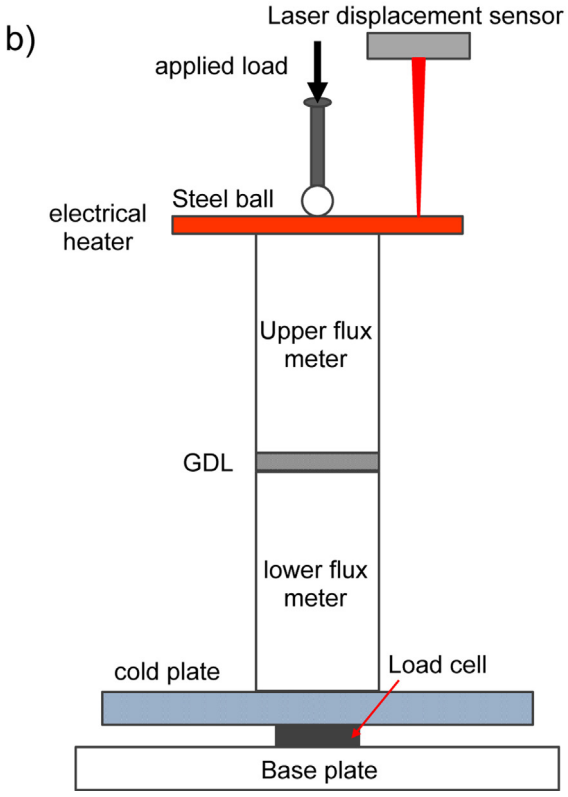

Fig. 8. (a) Photograph and (b) schematic view of experimental apparatus used for compression tests.

3.3. Uncertainty analysis

From stress definition, $\sigma = F/A$, uncertainties in the force and sample area measurements can cause uncertainty in the stress. The uncertainty of the stress–strain data, included in the plots, is calculated as follows [33]:

$$E(\sigma) = \sqrt{\left(\frac{E(F)}{F}\right)^2 + \left(\frac{E(A)}{A}\right)^2} \quad (13)$$

where, $E(\cdot)$ indicates the uncertainty of the parameters, F and A are the measured force and the sample area, respectively. Using load cell and the amplifier manufacturers' technical specifications, the uncertainty in the measured force was less than 1%. A circular cutter is used to cut the samples from the GDL sheets. The diameter of the cutter is about 1/16 of inch larger than the flux meters 1-inch diameter. Therefore, the area of the flux meters is determinant. The dimensions of the flux meters can change due to temperature

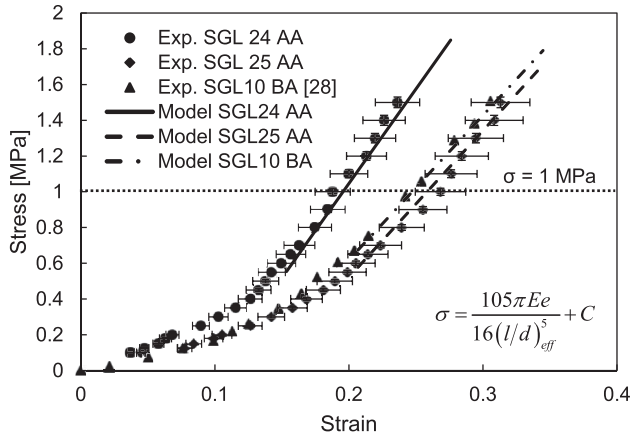

Fig. 9. Model results (lines) compared to experimental stress–strain data (points) for SGL 25 AA, 24AA, and 10BA [28] GDLs.

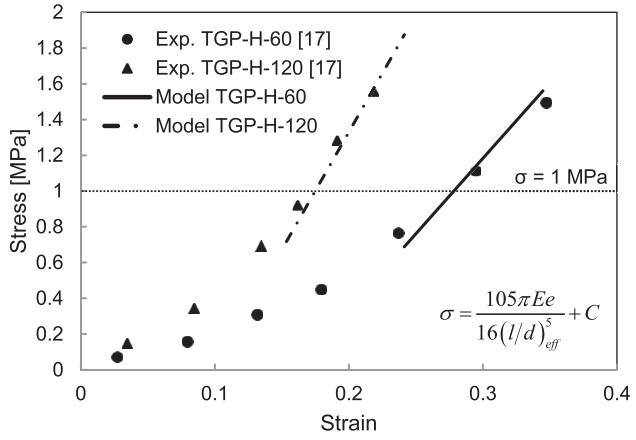

Fig. 10. Model results (lines) compared to experimental stress–strain data (points) for Toray TGP-H-060 and TGP-H-060 [17] GDLs.

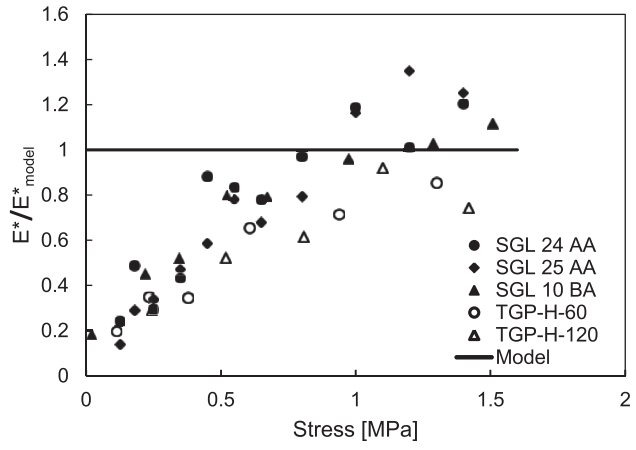

Fig. 11. The GDL through plane compressive deformation modulus versus stress.

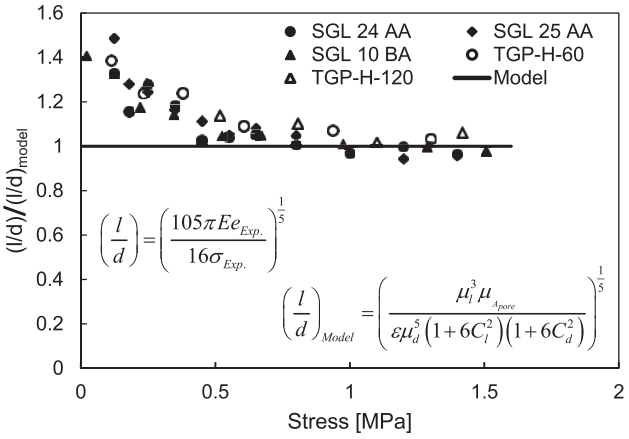

Fig. 12. The unit cell non-dimensionalized length factor versus stress.

variation during the experiments. Since, the temperature variations was not considerable, the area uncertainty is negligible.

For the strain, $\varepsilon = 1 - t'/t$, uncertainty sources are the deformed GDL thickness, t', measurement and the GDL initial thickness, t. The GDL thickness during deformation was measured using a laser displacement sensor that has a resolution of 0.005% of the measurement span based on the manufacturer technical data. Therefore, the strain uncertainty arises from displacement sensor is negligible. Another source is the GDL initial thickness variation, which is determined about ±7.89% according to the GDL's data sheet provided by the manufacturers. The uncertainty of the strain, included in the plots as well, is calculated as follows [33]:

$$E(\varepsilon) = \sqrt{\left(\frac{E(t')}{t'}\right)^2 + \left(\frac{E(t)}{t}\right)^2} \tag{14}$$

where, t' and t are the GDL compressed and initial thicknesses, respectively. Then, 7.89% uncertainty is calculated for the strain measurements.

4. Conclusion

In this paper, a novel analytical model was developed to predict the mechanical behavior of carbon fiber based GDLs under through plane compression. A unit cell approach was used to model the geometry of the GDL microstructure. Bending of carbon fibers was considered as the main mechanism responsible for the deformation of the GDL. The present model took into account salient GDL microstructural characteristics and properties such as carbon fiber diameter, elastic modulus, pore size distribution, and porosity. A comprehensive optical measurement study was performed to statistically determine effective geometric parameters needed in the proposed unit cell model. We measured compressive strain–stress for a number of commercially available SGL GDL samples. Comparison between the model results with the experimental stress–strain data showed that the present model could accurately predict the mechanical behavior of the GDL in the linear area, where the compressive pressures were higher than 1 MPa. Therefore, the model can be used for GDL deformation simulations as well as investigation of the GDL structural parameters (e.g. fibers diameter, pore size and porosity) effects on the mechanical behavior strength. It can also provide guidelines and engineering insight for manufacturing more efficient gas diffusion layers.

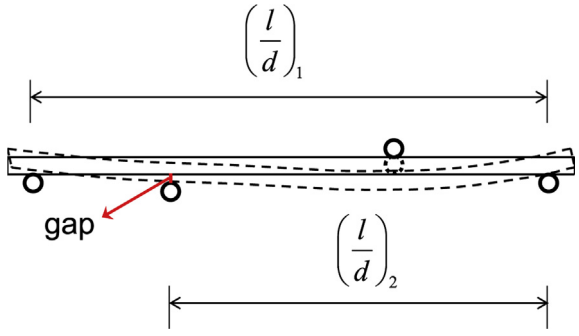

Fig. 13. Effect of the gap between fibers on the effective unit cell during the GDL compression (dashed lines show fiber location after GDL compression).

Appendix A

Using relationships reported by Mischke [32] for mean and standard deviation of simple algebraic operations on the independent random variables, the following equations can be written:

$$\mu_{xy} = \mu_x \mu_y \tag{A.1}$$

$$\mu_{x^4} = \mu_x^4\left(1 + 6C_x^2\right) \tag{A.2}$$

$$\mu_{\frac{1}{x^3}} = \frac{1}{\mu_x^3}\left(1 + 6C_x^2\right) \tag{A.3}$$

where, C is the coefficient of variation and can be calculated as

$$C_x = \frac{\widehat{\sigma}_x}{\mu_x} \tag{A.4}$$

where, μ and $\widehat{\sigma}$ are the mean and standard deviation, respectively. Considering Eqs. (A.1)–(A.3), μ_{d^4/l^3} can be written as

$$\mu_{\frac{d^4}{l^3}} = \mu_{d^4}\mu_{\frac{1}{l^3}} = \mu_d^4\left(1 + 6C_d^2\right)\frac{1}{\mu_l^3}\left(1 + 6C_l^2\right) \tag{A.5}$$

References

[1] P.A. García-Salaberri, M. Vera, R. Zaera, Int. J. Hydrogen Energy 36 (2011) 11856–11870.
[2] E. Sadeghi, N. Djilali, M. Bahrami, J. Power Sources 195 (2010) 8104–8109.
[3] A. Kusoglu, M.H. Santare, A.M. Karlsson, S. Cleghorn, W.B. Johnson, J. Electrochem. Soc. 157 (2010) B705.
[4] A. Kusoglu, A.M. Karlsson, M.H. Santare, S. Cleghorn, W.B. Johnson, J. Power Sources 161 (2006) 987–996.
[5] R. Solasi, Y. Zou, X. Huang, K. Reifsnider, D. Condit, J. Power Sources 167 (2007) 366–377.
[6] Z. Lu, C. Kim, A.M. Karlsson, J.C. Cross, M.H. Santare, J. Power Sources 196 (2011) 4646–4654.
[7] M.N. Silberstein, M.C. Boyce, J. Power Sources 196 (2011) 3452–3460.
[8] Y. Zhou, G. Lin, A.J. Shih, S.J. Hu, J. Power Sources 192 (2009) 544–551.
[9] A. Kusoglu, A.M. Karlsson, M.H. Santare, S. Cleghorn, W.B. Johnson, J. Power Sources 170 (2007) 345–358.
[10] S. Escribano, J.-F. Blachot, J. Ethève, A. Morin, R. Mosdale, J. Power Sources 156 (2006) 8–13.
[11] J. Kleemann, F. Finsterwalder, W. Tillmetz, J. Power Sources 190 (2009) 92–102.
[12] K.K. Poornesh, C.D. Cho, G.B. Lee, Y.S. Tak, J. Power Sources 195 (2010) 2718–2730.
[13] V. Radhakrishnan, P. Haridoss, Mater. Des. 32 (2011) 861–868.
[14] M.F. Serincan, U. Pasaogullari, J. Power Sources 196 (2011) 1314–1320.
[15] I. Nitta, T. Hottinen, O. Himanen, M. Mikkola, J. Power Sources 171 (2007) 26–36.
[16] E. Sadeghi, M. Bahrami, N. Djilali, J. Power Sources 179 (2008) 200–208.
[17] E. Sadeghi, N. Djilali, M. Bahrami, J. Power Sources 196 (2011) 246–254.
[18] H. Sadeghifar, M. Bahrami, N. Djilali, J. Power Sources 233 (2013) 369–379.
[19] I. Nitta, O. Himanen, M. Mikkola, Fuel Cells 8 (2008) 111–119.

[20] Z. Wu, S. Wang, L. Zhang, S.J. Hu, J. Power Sources 189 (2009) 1066–1073.
[21] Z. Wu, Y. Zhou, G. Lin, S. Wang, S.J. Hu, J. Power Sources 182 (2008) 265–269.
[22] Y. Zhou, G. Lin, A.J. Shih, S.J. Hu, J. Power Sources 163 (2007) 777–783.
[23] I. Nitta, O. Himanen, M. Mikkola, Electrochem. Commun. 10 (2008) 47–51.
[24] P. Zhou, C.W. Wu, G.J. Ma, J. Power Sources 159 (2006) 1115–1122.
[25] P. Zhou, C.W. Wu, G.J. Ma, J. Power Sources 163 (2007) 874–881.
[26] P. Zhou, C.W. Wu, J. Power Sources 170 (2007) 93–100.
[27] X.Q. Xing, K.W. Lum, H.J. Poh, Y.L. Wu, J. Power Sources 195 (2010) 62–68.
[28] I. Nitta, Inhomogeneous Compression of PEMFC Gas Diffusion Layers, Helsinki University of Technology, 2008.
[29] A. Tamayol, F. McGregor, M. Bahrami, J. Power Sources 204 (2012) 94–99.
[30] A. Tamayol, K.W. Wong, M. Bahrami, Phys. Rev. E 85 (2012) 026318.
[31] J. Shigley, C. Mischke, R. Budynas, Mechanical Engineering Design, eighth ed., McGraw-Hill, 2006.
[32] C.R. Mischke, Mathematical Model Building, Iowa State University Press, 1980.
[33] J.R. Taylor, An Introduction to Error, University Science Books, Sansalito, 1997.
[34] M. Mathias, J. Roth, J. Fleming, W. Lehnert, Handbook of Fuel Cells, John Wiley & Sons, 2003.